J. COMBIN. MATH. COMBIN. COMPUT. 127a (2025) 743–763

Journal of Combinatorial Mathematics
and Combinatorial Computing
www.combinatorialpress.com/jcmcc

Combinatorial Press

Algorithm Optimisation and Landslide Risk Assessment for Critical Soil Thickness Calculation on Slopes Based on 3D Numerical Simulation (FLAC-3D) and Geographic Information System (GIS)

Lida Wang[1], Yuqiong He[1], Yongqi Wang[1,✉], Yunxi Zhao[1]

[1] *Faculty of Transportation Engineering, Kunming University of Science and Technology, Kunming, Yunnan, 650500, China*

ABSTRACT

This study focuses on the Dingjiafen slope in Chuxiong City, China, with the aim of improving the accuracy of slope landslide risk prediction. Formulas for calculating the critical soil layer thickness at the onset of slope instability are derived based on the physical model of the slope. Using the Digital Elevation Model (DEM) and ArcGIS, the critical and maximum soil layer thickness of each slope unit are calculated to predict potential landslide areas. FLAC-3D is employed to simulate and analyze the slope's stability under natural conditions, and the numerical simulation results are compared with the predictions in ArcGIS. The findings reveal variations in the critical and maximum soil layer thickness among different slope units due to diverse topography. The slope units on both sides of the Chumeng Highway slopes, with a critical soil layer thickness (D_{cr}) between 1 and 3 meters, are connected, aligning with the results of FLAC-3D three-dimensional numerical simulation and the actual sliding positions on-site. Applying this method to simulate the soil layer thickness at the critical state for each slope unit enables slope stability prediction, offering a new perspective for the analysis and prediction of slope stability.

Keywords: critical soil layer thickness, maximum soil layer thickness, slope stability, prediction

1. Introduction

Due to the increasing occurrences of slope instability events caused by natural and anthropogenic factors [1], especially the emergence of large and giant landslides, significant threats and losses to human life and property have been pose [2]. This seriously affects people's lives, transportation, and the safe operation of infrastructure, and has adverse effects on the environment [3]. China is one of the countries most prone to geological disasters, with 5,659 geological disasters in 2022, including 3,919 landslides, accounting for 69.3% [4]. Therefore, it is necessary to analyze and predict the stability of slopes [5].

✉ Corresponding author.
E-mail address: wanglida@stu.kust.edu.cn (Y. Wang).

Received 01 June 2024; Revised 11 October 2024; Accepted 11 December 2024; Published Online 15 April 2025.
DOI: 10.61091/jcmcc127a-043

In the field of slope stability prediction, significant achievements have been made through the use of physical models and numerical simulations [6-10]. For instance, the combination of physical models and the substitution of surface watershed area for subsurface water flow in slope stability prediction has successfully identified the positions of landslides and potential landslides [11-13]. The application of a quasi-dynamic moisture index model to simulate the stable state of slope surfaces has shown good results in practical applications [14-15]. Researchers have further proposed a landslide hazard prediction hydro-mechanical coupling model considering the quasi-dynamic moisture index [16], used for regional landslide prediction, revealing the success of the quasi-dynamic moisture index model in unstable analysis under critical rainfall conditions [17]. In addition, some studies have combined terrain index models and infinite slope stability models [15] [18-20], achieving satisfactory results in landslide prediction for slope watershed areas.

Current research mostly focuses on the consideration of physical and hydrological models in slope stability analysis and prediction, with less attention to the complex factors of the slope's own geological structure, soil thickness, and the role of rainfall in the slope. When considering the influence of soil thickness on slope stability, some studies emphasize the strong linear relationship between soil thickness and slope gradient [21], while others investigate the impact of soil thickness on surface seepage by setting different soil thicknesses in experiments [22]. As slope soil thickness, surface, and bedrock topography directly affect the flow path of groundwater and the initiation of landslides [13]. Therefore, based on considerations of slope gradient, watershed area, and surface coverage, this paper aims to focus on discussing the critical soil thickness at the critical state of slope instability and its impact on slope stability. It utilizes geological survey data to establish surface and bedrock DEM, models and verifies the feasibility of the critical soil thickness model, and provides a new research perspective for in-depth analysis of slope stability through coupling multiple sources of slope data.

2. Study area

The study area is located at longitude 101°02′ east and latitude 24°13′ north, K64+200 of the Chumeng Highway, southwest of Dingjiafen Village, Shuangbai County, Yunnan Province, approximately 7 kilometers from Shuangbai County. The natural terrain has a slope ranging from 15° to 25°, and the elevation of the slope is between 1752.5 and 1875 meters. Some local slope units are steep, with a maximum height difference of 100 meters, as shown in Figure 1. The area belongs to the subtropical plateau monsoon climate zone, with distinct wet and dry seasons, an average annual temperature of 15°C, and an annual rainfall of 700-800mm. Dingjia River is located at the forefront of the slope, but its impact on slope stability is relatively small. There are no other large surface water systems except for Dingjia River. Groundwater mainly exists in the residual slope deposit layer of the Quaternary, including angular gravelly clay, gravel layer, and bedrock fractures. In some local sections, influenced by the terrain, the flow direction is basically consistent with the slope direction.

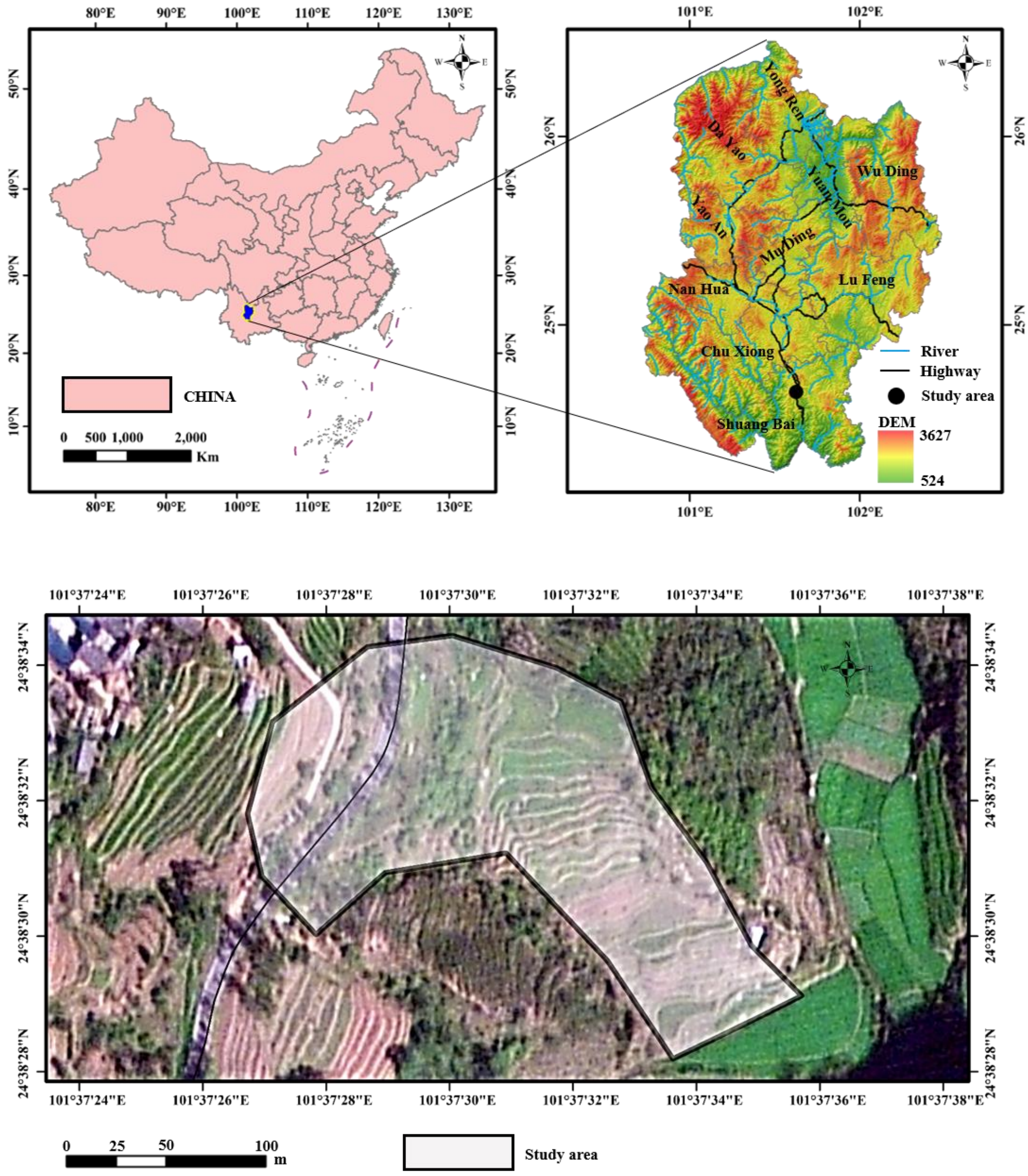

Fig. 1. Study area

The selected area outlined in purple dashed lines is the research site, consisting of two potential landslides, H1 and H2. The dark blue solid line in the upper left represents the location of the Chumeng Highway. The potential sliding directions of landslides H1 and H2 are indicated by arrows, aligned with the flow direction of the Dingjia River.

The drilling data show that

1) 0-1.2m is artificial fill, brownish grey, brownish yellow, purple-red, composed of gravel, crushed bricks and clay;

2) 1.1m- 11.50m is residual slope deposits, brownish red, purple-red with angular gravelly chalky clay, angular gravelly clay;

3) 11m-30m is the upper section of Jurassic Upper Toudian Formation with purple-red and grey mudstones interbedded with siltstones, of which the middle and upper part of the landslide are dominated by purple-red, and the lower part is grey and purple-red. The upper part of the landslide is mainly purple-red, and the lower part is grey, purple-red, and according to the physical and mechanical properties and the degree of weathering, it is classified into fully weathered mudstone with siltstone, strongly weathered mudstone with siltstone, and moderately weathered mudstone with siltstone, as shown in Figure 4 and Figure 5, and the location of the boreholes is shown in Figure 3.

The geomorphological survey of the study area revealed that the road surface of the Chumeng Highway, located above H1, had subsided and cracked, the trees beside the highway had been significantly displaced and tilted, and the rim of a well in the study area, H2, had been significantly cracked (Figure 2), which suggests that there is a potential for sliding between H1 and H2.

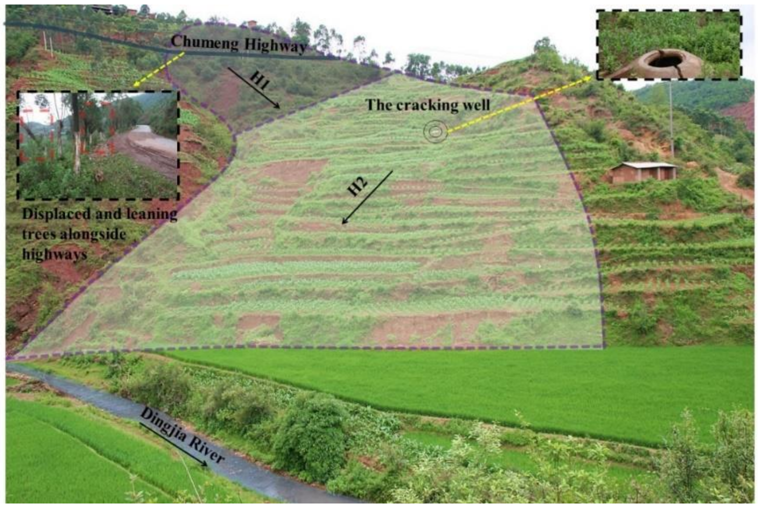

Fig. 2. Slope schematic

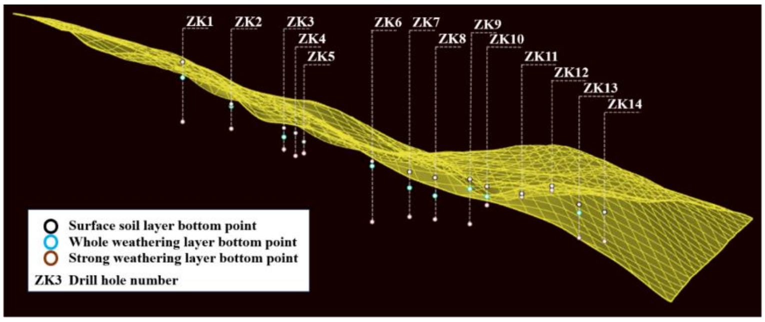

(a)

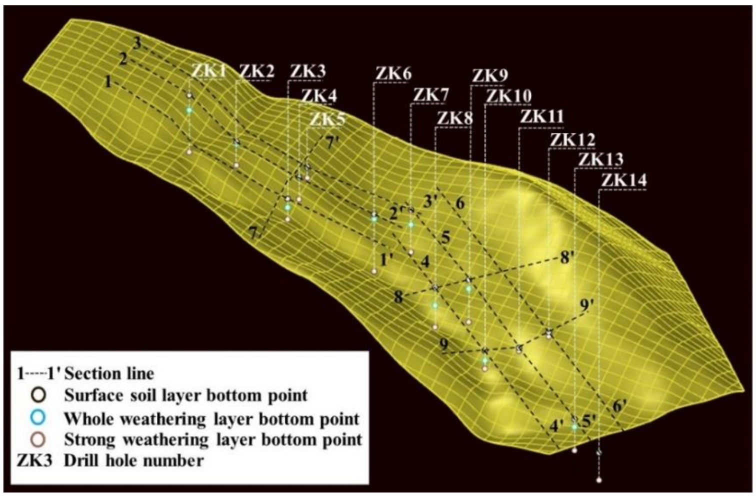

(b)

Fig. 3. Borehole distribution map

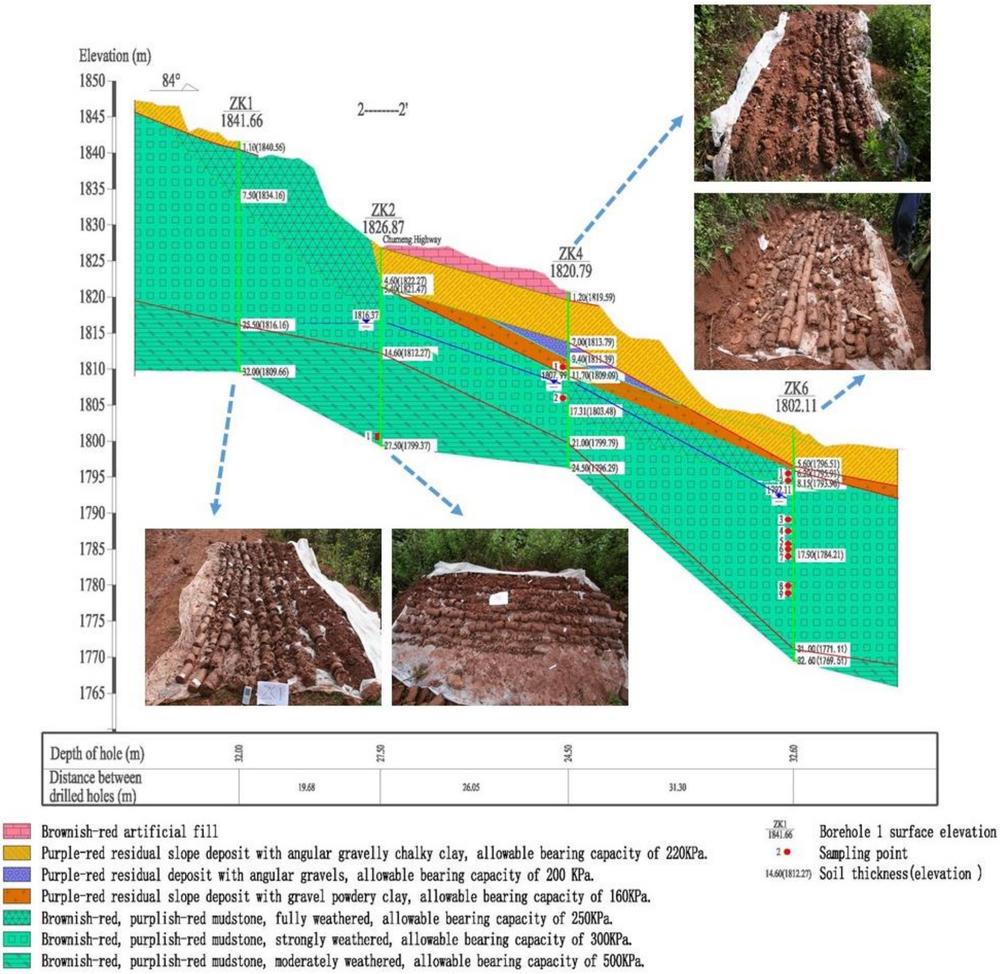

Fig. 4. 2-2' Cross-sectional geological profile

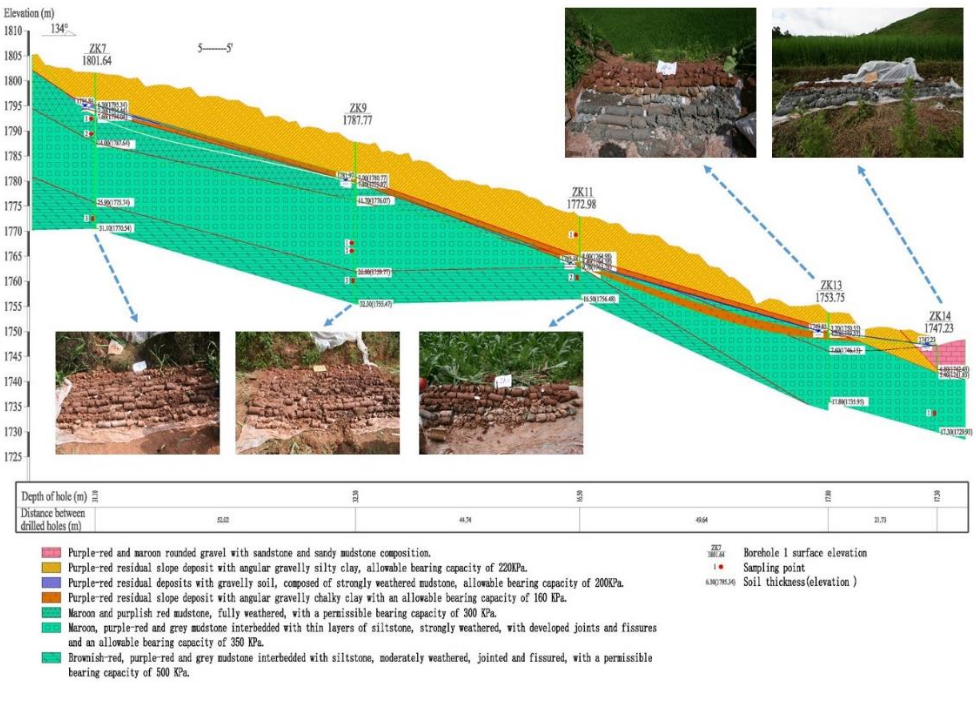

Fig. 5. 5-5' Cross-sectional geological profile

3. Critical Soil Thickness Model for Slope Instability

The analysis and prediction of slope stability in this paper require consideration of relevant data such as slope topography, slope gradient, upslope watershed area, surface coverage, soil thickness, and its characteristics. Surface topography, slope gradient, and upslope watershed area can be extracted from DEM models, while surface coverage can be obtained through field surveys. However, obtaining information about the bedrock topography is relatively challenging. Therefore, based on exploration drilling data, this paper reflects the surface topography of the slope bedrock based on the thickness data of slope surface and drilling holes, and obtains information about the geological strata and physical-mechanical properties of the slope rock-soil through field surveys and relevant indoor experiments.

Two main controlling factors affecting slope stability due to terrain are groundwater flow convergence and surface slope. Groundwater convergence causes a rise in the water table, increasing pore water pressure and leading to landslides. The occurrence of landslides often happens in the downhill direction of groundwater flow convergence. Soil thickness is the thickness between the bedrock surface and the ground surface, mainly influencing the distribution path of rainfall and the depth of the saturated soil layer, as shown in Figure 6.

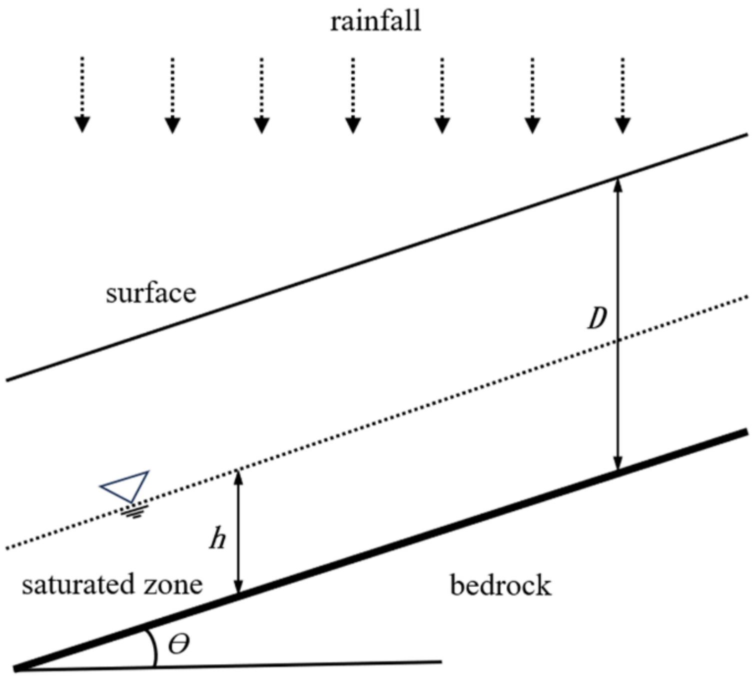

Fig. 6. Slope structure schematic

Where D is the thickness of the soil in the vertical direction, in meters, h is the depth of the groundwater level above the sliding surface in meters, θ is the slope angle of the ground surface in degrees.

3.1. *Physical Mechanics Model*

The influence of unsaturated and saturated groundwater flow in slopes is significant, and it is also constrained by factors such as topography, soil thickness, hydraulic characteristics, etc. To analyze the impact of topography and soil thickness on the slope, assuming the presence of an unsaturated soil layer (or weathering layer) above the bedrock, based on the Mohr-Coulomb instability law and stability analysis of an infinite slope, and considering the effect of dynamic water pressure, the slope stability factor is given by

$$F_s = \frac{F_R}{F_D} = \frac{c + (\sigma - u) \cdot \tan\varphi}{\tau + W_D} = \frac{c + \left(\left((D-h)\gamma_t + h\gamma_s\right) - h\gamma_w\right) \cdot \cos^2\theta \tan\varphi}{\left((D-h)\gamma_t + h\gamma_s\right)\sin\theta\cos\theta + h\gamma_w \sin\theta\cos\theta} \tag{1}$$

Where F_R is the resistance to sliding force, F_D is the downward force, c is the cohesion of the soil in KN/m², σ is the total normal stress in KN/m², u is the pore water pressure in KN/m², φ is the internal friction angle in degrees, θ is the slope angle of the ground surface in degrees, γ_s is the saturated soil unit weight in KN/m³, γ_t is the unit weight of unsaturated soil. γ_w is the unit weight of water, D is the thickness of the soil in the vertical direction, in meters, h is the depth of the groundwater level above the sliding surface in meters, W_D is the dynamic water pressure, $W_D = \gamma_w hI\cos\theta$, where I is the hydraulic gradient, $I = \sin\theta$.

3.2. *Critical Soil Layer Thickness Model*

When the slope stability factor ($F_s = 1$), the slope element will be in a critical state of instability. The groundwater level (h) above the sliding surface is determined by rearranging Equation (1).

$$h = \frac{c - D\gamma_t \cdot \cos^2\theta\left(\tan\theta - \tan\varphi\right)}{\cos^2\theta\left(\left(\gamma_s - \gamma_t\right)\left(\tan\theta - \tan\varphi\right) + \gamma_w\left(\tan\varphi + \tan\theta\right)\right)} \tag{2}$$

At this point, the groundwater level (h) is the critical groundwater level (H_{cr}) when the slope is in the state of landslide initiation (Borga, M. et al. 1998), as shown in Figure 6.

When the slope soil thickness (D) is equal to the critical groundwater level (H_{cr}), the slope soil is in a saturated zone state. At this point, the soil thickness (D) is the critical soil layer thickness (D_{cr}), i.e., ($h = H_{cr} = D = D_{cr}$). Equation (2) can be written as

$$D_{cr} = \frac{c}{\cos^2\theta\left(\gamma_s\left(\tan\theta - \tan\varphi\right) + \gamma_w\left(\tan\varphi + \tan\theta\right)\right)} \tag{3}$$

The symbols in the equation have the same meanings as in Equation (1).

3.3. *Model of Maximum Soil Layer Thickness*

Under steep terrain slope conditions, sliding may occur even in the absence of saturated water flow in the slope soil layer. In equation (3), this is specifically manifested by the absence of the term $\gamma_w\left(\tan\varphi + \tan\theta\right)$ in the denominator, and the soil unit weight is the unsaturated unit weight. In this case, the thickness of the slope soil layer reaches the upper limit of the critical soil layer thickness, namely the maximum soil layer thickness (D_{max}).

$$D_{max} = \frac{c}{\gamma_t \cos^2\theta\left(\tan\theta - \tan\varphi\right)} \tag{4}$$

The symbols in the equation have the same meanings as in equation (1). The thickness of the slope soil layer is related to the cohesion, internal friction angle of the soil, and the slope gradient of the terrain. As indicated in equation (4), the soil layer thickness decreases with an increase in the terrain slope. This well explains why the soil layer thickness is thinner on steeper slopes, and even exposes rock formations.

4. Soil Thickness Calculation and Slope Stability Analysis Based on ArcGIS

4.1. *Extraction of Terrain Feature Data*

By utilizing actual surveyed topographic data of the slope and slope borehole survey data, Triangulated Irregular Network (TIN) interpolation method is employed in ArcGIS to generate corresponding 1m×1m

DEM units. The terrain, slope, upslope contributing area, etc., of each slope unit can be calculated and extracted from the corresponding DEM. The physical properties and mechanical indicators of the rock and soil mass between the soil layer, weathered weak rock layer, and the instability surface of the bedrock are obtained. The critical soil layer thickness (D_{cr}) and maximum soil layer thickness (D_{max}) when the slope unit experiences sliding are studied. The permeability coefficient of the soil is $K = 1\times10^{-4}$ m/s, and relevant parameters such as soil cohesion, internal friction angle, etc., are provided in Table 1.

Table 1. Related Parameters

C_s [KN/m2]a)	φ [°]b)	γ_s [KN/m3]c)	γ_t [KN/m3]d)	γ_w [KN/m3]e)
15.8	28.7	25.38	19.6	9.8

a) Cohesive strength of soil; b) Internal friction angle; c) Saturated unit weight of soil; d) Unsaturated unit weight of soil; e) Unit weight of water.

Using ArcGIS to generate the slope DEM, as shown in Figure 7, there are two landslide directions on the downslope of the Chumeng Highway, namely the H1 landslide and H2 landslide. Through investigation, it was found that the deformation of the H1 and H2 landslides is evident, with local sliding already occurring. Tension cracks within the sliding body, rupture cracks at the rear of the landslide, and shear tension cracks on both sides have developed, and the perimeter cracks of the landslide are interconnected.

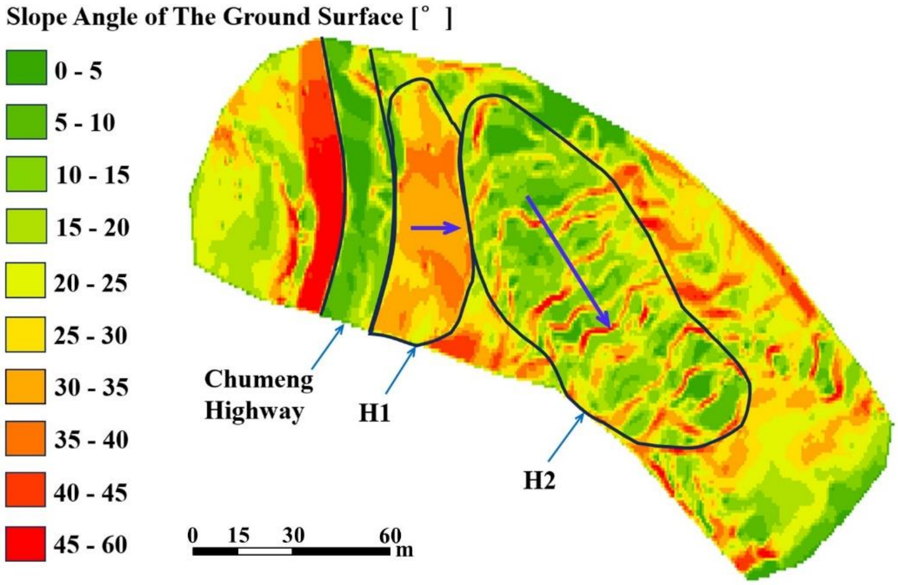

Fig. 7 Slope surface gradient

The blue arrows indicate the locations of the Chumeng Highway and potential landslides H1 and H2. The purple arrows represent the potential sliding directions of the landslides.

4.2. Analysis of Critical Soil Layer Thickness for Landslide

Based on the physical and mechanical indicators of the slope and its rock-soil mass, the critical soil layer thickness (D_{cr}) and the maximum soil layer thickness (D_{max}) calculated using equations (3) and (4) are shown in Figure 8. The D_{cr} curve under saturated conditions and the D_{max} curve under unsaturated conditions are significantly influenced by the cohesion and internal friction angle of the slope soil layer. Different cohesion and internal friction angles result in different D_{cr} and D_{max} curves. Under the same topographical conditions, the maximum soil layer thickness (D_{max}) is greater than the critical soil layer thickness (D_{cr}).

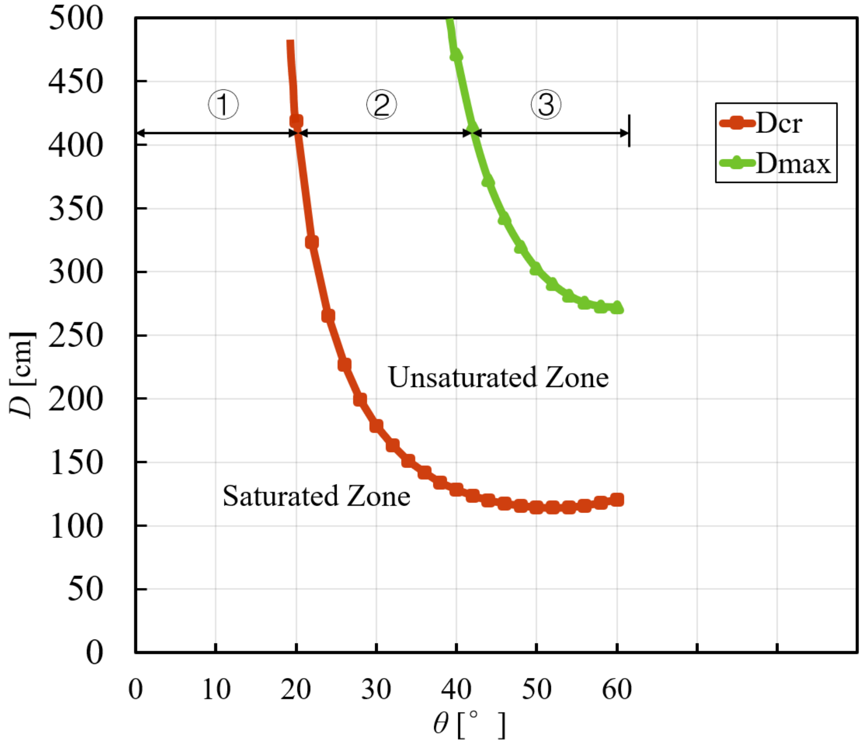

Fig. 8. Hyperbolic curve graph of soil layer Thickness

The horizontal axis represents the slope gradient, and the vertical axis represents the soil layer thickness. In Figure 8, in the region marked as ① within the saturated zone, where the slope soil layer thickness is less than the critical soil layer thickness, even though the slope soil layer is entirely in a saturated state, shallow landslides will not occur. This area is considered a conditionally stable zone. In the region marked as ② within the unsaturated zone, where the slope soil layer thickness is between the critical soil layer thickness and the maximum soil layer thickness, shallow landslides will be triggered under the influence of rainfall. In the region marked as ③ within the completely unsaturated zone, this area is unconditionally unstable, and sliding will occur regardless of the presence of saturated water flow in the slope. However, it is generally difficult for the slope soil layer thickness to reach the maximum soil layer thickness.

By substituting soil characteristics and relevant topographic data into equations (3) and (4), using ArcGIS software to simulate the critical soil layer thickness and maximum soil layer thickness of the slope, the calculated results are shown in Figure 9 and Figure 10. The critical soil layer thickness and maximum soil layer thickness at any point on the slope in a critical sliding state can be presented in the figures. Due to variations in the terrain and slope of each slope unit, the soil layer thickness at which each unit is in a critical sliding state is inconsistent. In this study, the slope's critical and maximum soil layer thickness is displayed in increments of 0.5m.

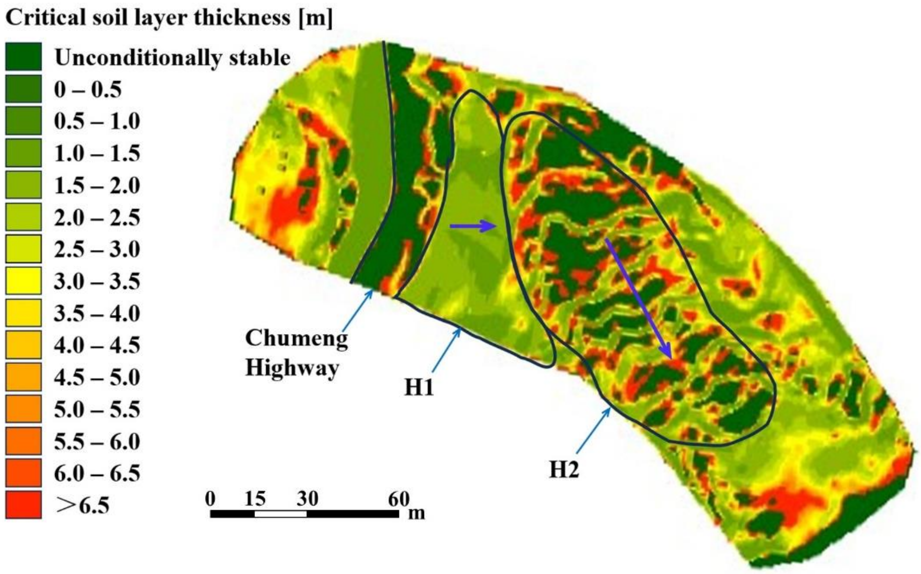

Fig. 9. Landslide critical soil layer thickness (D_{cr})

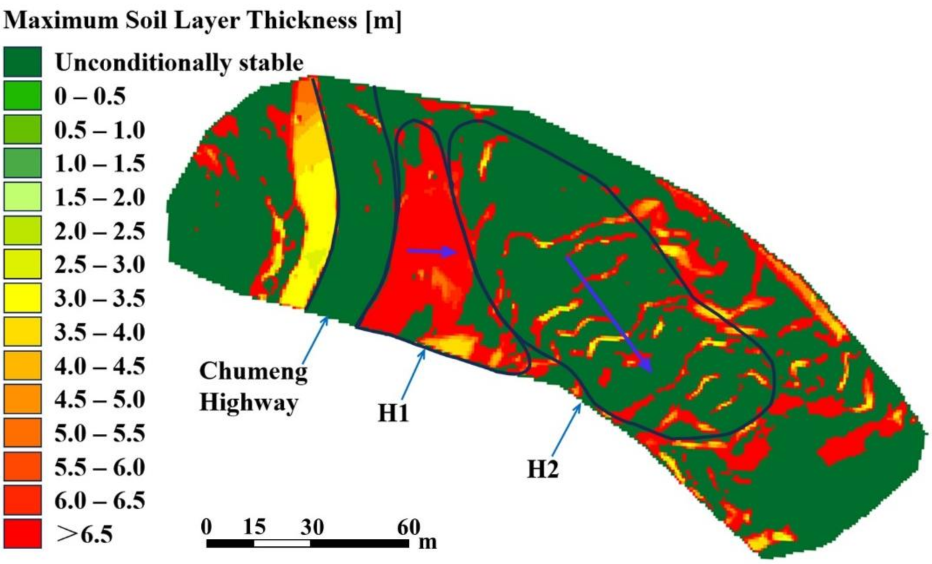

Fig. 10. Landslide maximum soil layer thickness (D_{max})

Figure 9 shows the critical soil layer thickness (D_{cr}) calculated for each point on the slope under saturated conditions. The terrain slope between 0 to 5 degrees is relatively gentle, corresponding to the slope units in region ① in Figure 8. This region is considered a conditionally stable area and is unlikely to experience shallow landslides, although the possibility of an overall slope-induced landslide cannot be ruled out. Slope units with critical soil layer thickness (D_{cr}) between 1 to 3 meters are located on both sides of the Chumeng Highway, precisely at the positions where on-site landslide displacement occurs. Figure 9 shows a tendency of connected slope units in the H2 landslide area with critical soil layer thickness (D_{cr}) greater than 0.5. Under certain rainfall conditions, these slope units may experience sliding influenced by both the H1 landslide and its own gravity.

Figure 10 shows the maximum soil layer thickness (D_{max}) calculated for each point on the slope under unsaturated conditions. Similar to Figure 9, the terrain slope between 0 to 5 degrees is relatively gentle, corresponding to the slope units in region ① in Figure 8. This region is considered a conditionally stable area and is unlikely to experience shallow landslides, although the possibility of an overall slope-induced landslide cannot be ruled out. The slope units with maximum soil layer thickness (D_{max}) between 1.5 to 5.5 meters are located on both sides of the Chumeng Highway, precisely at the positions where on-site landslide displacement occurs.

As indicated by equations (3) and (4), the critical soil layer thickness (D_{cr}) and the maximum soil layer thickness (D_{max}) are influenced by the cohesion and internal friction angle of the slope soil mass. Conversely, the curve states of (D_{cr}) and (D_{max}) will also alter the cohesion and internal friction angle of the slope soil mass.

When using the (D_{cr}) curve under saturated conditions and the (D_{max}) curve under unsaturated conditions to calculate the internal friction angle and cohesion of the slope soil mass, the distribution of soil layer thickness is highly sensitive to the slope gradient and related parameters. If the (D_{cr}) and (D_{max}) curves of the soil layer change, the cohesion and internal friction angle of the soil layer thickness will also change with variations in the slope gradient. This is closely related to changes in the topography, indicating a strong correlation between slope terrain and (D_{cr}) and (D_{max}) curves. Additionally, the thickness of the slope soil layer depends on the terrain between the slope surface and the bedrock surface. The morphology of the sliding zone-bedrock interface is a crucial factor controlling the connectivity of the saturated area. The sliding surface of the landslide is greatly influenced by pore water pressure and the topography of the bedrock surface.

4.3. *Criteria for Landslide Assessment*

Based on the analysis in Section 4.2, assuming cohesion ($c > 0$), the occurrence of landslides on a slope is related to the topography of the slope surface.

1) When the soil layer thickness ($D < D_{cr}$), as the water level of saturated flow cannot be higher than the ground surface, the depth (h) of saturated flow cannot meet the requirements of the critical groundwater depth (H_{cr}). In this case, even heavy rainfall will not cause shallow landslides, but it may result in saturated surface runoff.

2) When the soil layer thickness ($D > D_{cr}$) and ($D < D_{max}$), the rise in groundwater level due to rainfall, if it exceeds the critical groundwater level (H_{cr}), can lead to landslides.

3) For steep slopes, if the internal friction angle ($\varphi < \theta$) (slope gradient), the critical groundwater level (H_{cr}) decreases linearly with increasing soil layer thickness until it reaches 0. This implies that even though there is no saturated flow on the slope, if the soil layer thickness on the slope reaches the upper limit (D_{max}) of the critical soil layer thickness, shallow landslides may occur. However, it is rare for slope soil layers to reach the upper limit (D_{max}) because periodic rainfall always generates some saturated groundwater flow, destabilizing the slope when the soil layer thickness is less than (D_{max}).

4) For relatively gentle slopes, if ($\varphi > \theta$), the critical groundwater level (H_{cr}) increases linearly with increasing soil layer thickness, and there is no issue of an upper limit soil layer thickness (D_{max}).

5) On slopes with zero cohesion, if the slope gradient ($\theta > \varphi$), it is impossible to form a soil layer on the slope. If ($\theta < \varphi$), even with a thin layer of soil, the slope is extremely unstable because in this case, even light rain can provide enough saturated water depth (H_{cr}) to trigger a landslide.

From the above analysis, it is evident that the soil layer thickness is a crucial indicator in slope stability analysis. Situations where the soil layer thickness is greater than the maximum soil layer thickness are uncommon, and landslides are more likely to occur when the slope's soil layer thickness is between (D_{cr}) and (D_{max}).

5. Numerical Simulation Analysis Based on FLAC-3D

5.1. *Establishment of a Three-Dimensional Model for the Slope*

From the computational analysis in Section 4.2, it can be seen that the slope gradient and soil layer thickness are two crucial factors affecting slope stability. To visually observe their impact on slope stability, a true three-dimensional model of the research site was established for analysis. According to the geological survey report, there are a total of 14 boreholes distributed at the study area based on the characteristics of the landslide body, as shown in Figure 3 (a, b).

Based on the data from geological exploration, contour maps of different strata were obtained using the Kriging spatial interpolation method in Surfer software. This method transforms the measured data of discrete points into a continuous spatial surface. Kriging interpolation is a technique that predicts the values of other points ($\hat{E}S_0$) by assigning weights to known sample points. The formula for Kriging interpolation is

$$\hat{E}S_0 = \sum_{i=1}^{n} w_i Z(S_i) \tag{5}$$

where $Z(S_i)$ is the measured attribute value at the i th location, w_i is the weight of the measured value at the i th location, S_0 is the location to be interpolated, n is the number of known sample points.

Using Rhino and FLAC-3D modeling software, the distribution of soil layers and the position of the landslide body are presented in the true three-dimensional model of the slope, as shown in Figure 11.

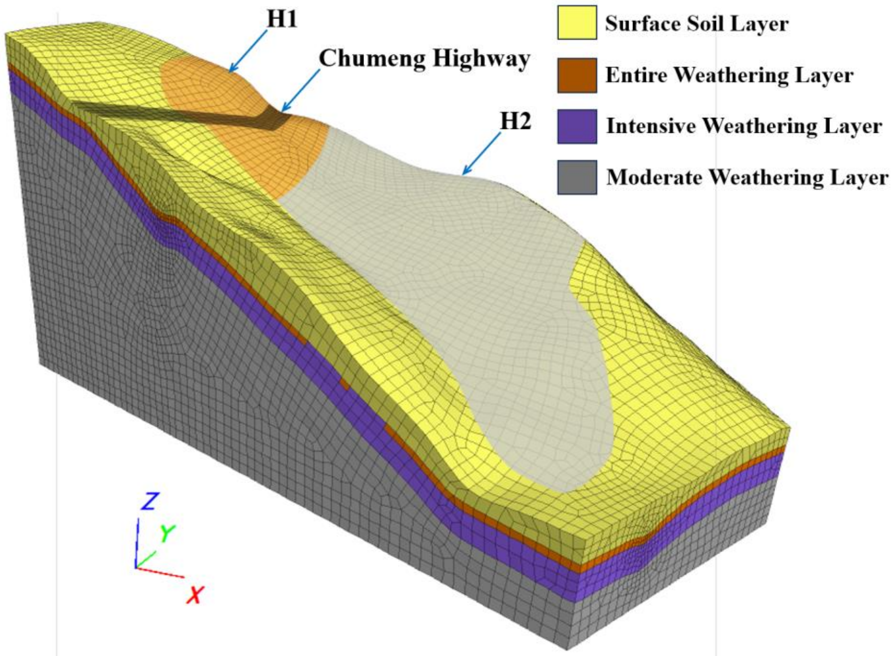

Fig. 11. Three-dimensional model of slope mass

5.2. Division of the Study Area Based on the Average Thickness of the Surface Soil Layer

Based on geological exploration data, exploration points adjacent to the positions of the H1 and H2 landslides with similar surface soil thickness are divided into regions. A total of 14 exploration points are divided into 5 regions, with regions 1 and 2 forming the H1 landslide and regions 3, 4, and 5 forming the H2 landslide, as shown in Figure 12. The average thickness of the surface soil layer in each region is presented in Table 2, the physico-mechanical indices of each soil layer are shown in Table 3, and the parameters of each soil layer selected for numerical simulation of the 3D model in FLAC-3D are shown in Table 4.

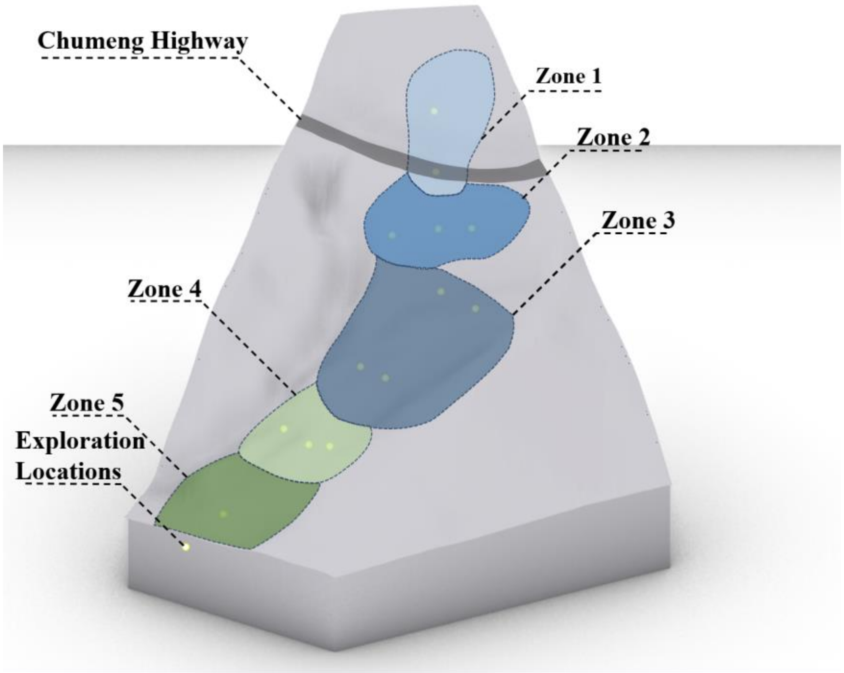

Fig. 12. Research area division map

Table 2. Exploration site Area Division

Zone Code	1	2	3	4	5
Exploration Site Code	ZK1 ZK2	ZK3 ZK4 ZK5	ZK6 ZK7 ZK8 ZK9	ZK10 ZK11 ZK12	ZK13 ZK14
Average Thickness of Surface Soil Layer in the Zone [m]	2.85	11.63	7.15	6.03	4.80

Table 3. Statistical table of physical and mechanical indicators for each soil layer

Soil type	lithology	Drill hole number	Depth of extraction (m)	Dry density ρ (g/cm3)	Cohesion C (KPa)	Angle of internal friction φ (°)
Surface soil layer	Silty clay	ZK11-1	3.70-3.90	1.66	15.8	25.3
		ZK12-1	3.30-3.50	1.64	18.3	20.8
		Average value		1.65	17.05	23.05
	Silty clay	ZK4-1	10.50-10.70	1.81	7.8	31.3
		ZK12-2	4.30-4.50	1.60	17.1	19.4
		Average value		1.71	12.45	25.35
Fully weathered soil layer	Fully weathered mudstone	ZK8-1	7.10-7.30	1.81	7.2	31.2
		ZK8-2	12.60-12.80	1.84	18.9	29.5
		ZK6-1	6.60-6.80	1.88	11.3	30.7
		ZK6-2	7.60-7.80	1.80	12.4	28.7
		ZK6-3	13.00-13.20	1.75	20.1	26.2
		ZK6-4	14.60-14.80	1.78	18.2	27.5
		ZK6-5	16.40-16.60	1.82	11.9	30.5
		ZK6-6	17.10-17.30	1.80	17.2	27.5

		ZK7-1	9.20-9.40	1.90	11.8	30.3
		ZK7-2	12.20-12.40	1.91	10.7	31.8
		ZK10-1	5.70-5.90	1.76	9.3	31.8
		Count		11	11	11
		Maximum values		1.91	20.1	31.8
		Minimum value		1.75	7.2	26.2
		Average value		1.82	13.5	29.6
		Standard deviation		0.05	4.10	1.81
		Coefficient of variation		0.03	0.30	0.06
		Correction factor		1.02	0.83	0.97
Strongly weathered soil layer	Strongly weathered mudstone	ZK3-1	14.20-14.40	1.76	9.5	29.2
		ZK3-2	15.10-15.30	1.82	8.3	30.3
		ZK4-2	14.80-15.00	1.86	6.2	32.5
		ZK9-1	20.10-20.30	1.96	8.1	32.3
		ZK9-2	21.70-21.90	1.87	10.4	31.5
		ZK6-7	18.10-18.30	1.92	11	31
		ZK6-8	22.50-22.70	1.8	15.8	27.4
		ZK6-9	23.00-23.20	1.88	8.9	31.8
		ZK6-10	25.10-25.30	1.89	10	30.8
		Count		9	9	9
		Maximum values		1.96	15.8	32.5
		Minimum value		1.76	6.2	27.4
		Average value		1.9	9.8	30.8
		Standard deviation		0.06	2.51	1.53
		Coefficient of variation		0.03	0.26	0.05
		Correction factor		1.02	1.16	1.03

Table 4. Selected parameters for FLAC-3D numerical simulation

Soil type	lithology	Dry density ρ (g/cm3)	Cohesion C (KPa)	Angle of internal friction φ (°)	Elastic modulus E (MPa)	Poisson's ratio μ
Surface soil layer	Silty clay	1.68	14.80	24.20	11000	0.30
Fully weathered soil layer	Fully weathered mudstone	1.82	13.55	29.61	15000	0.25
Strongly weathered soil layer	Strongly weathered mudstone	1.86	9.80	28.02	20000	0.30
Bedrock	-	2.66	680	41.77	20000	0.25

5.3. *Displacement Field Analysis under Natural Conditions*

Numerical simulation calculations of the displacements generated on the slope under natural conditions, solely influenced by gravity, were conducted using FLAC-3D. The displacement contour maps in the X, Y, and Z directions of the slope body can be obtained (Figure 13, Figure 14, Figure 15), along with the total displacement contour map (Figure 16).

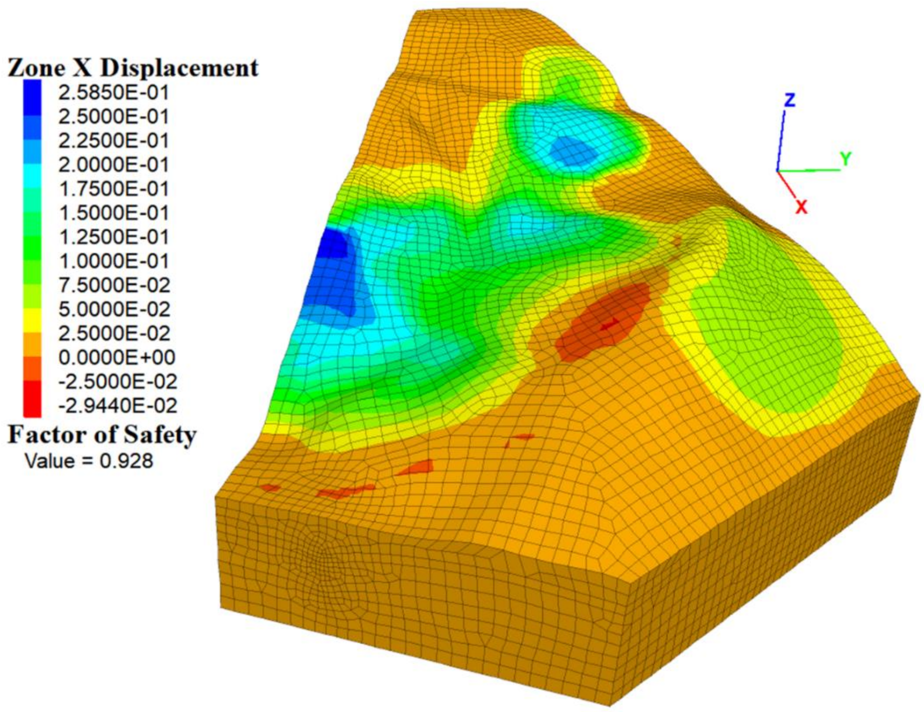

Fig. 13. Landslide X-direction displacement cloud map

The displacement contour map in the X-direction shows that in zone 1, there is a displacement of 2.5–10 cm in the positive X-axis direction. In zone 2, the displacement is 5–22.5 cm in the positive X-axis direction. In zone 3, where most areas are located in low-lying valleys, the displacement along the positive X-axis direction is 5–20 cm. Some areas, appearing in orange and red, are situated along the ridge line. There is a trend of movement towards the middle valley direction along the negative X-axis, with a displacement magnitude of 2–3 cm. In zone 4, the displacement along the positive X-axis direction is 5–20 cm, while in zone 5, the displacement ranges from 0 to 10 cm along the positive X-axis. The locations with larger X-direction displacements are mainly concentrated in zones 2, 3, and 4.

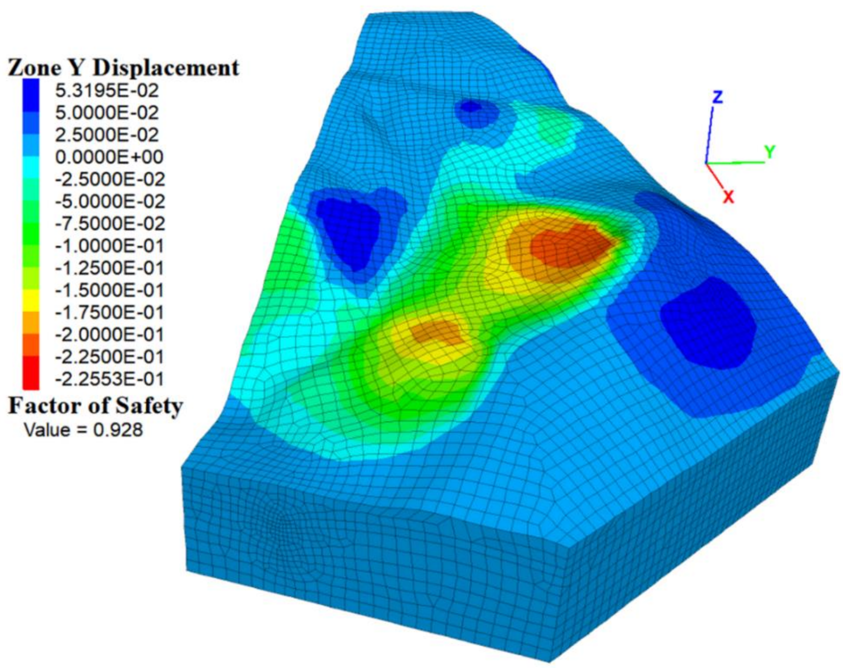

Fig. 14. Landslide Y-direction displacement cloud map

The displacement contour map in the Y-direction shows that in zone 1, there is a displacement of 0–5 cm in the positive Y-axis direction. In zone 2, most areas have a displacement of 2.5–10 cm in the negative Y-axis direction. In zone 3, the displacement along the negative Y-axis direction is 5–22.5 cm. In zone 4, the displacement along the negative Y-axis direction is 5–20 cm, and in zone 5, the displacement ranges from 0 to 5 cm in the negative Y-axis direction. Similar to the X-direction, locations with larger Y-direction displacements are concentrated in zones 2, 3, and 4.

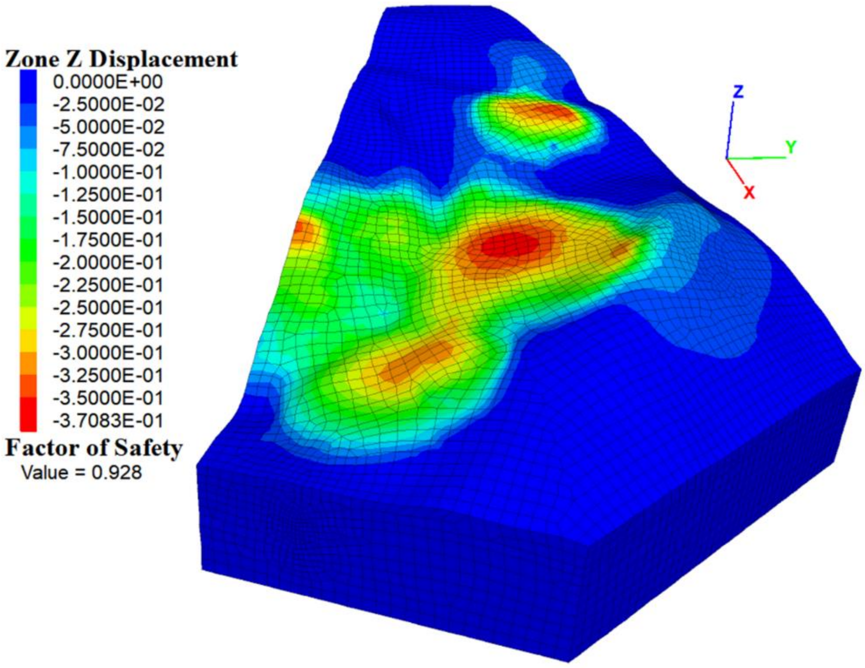

Fig. 15. Landslide Z-direction displacement cloud map

The displacement contour map in the Z-direction shows that in zone 1, there is a displacement of 0–12.5 cm in the negative Z-axis direction. In zone 2, the displacement along the negative Z-axis direction is 2.5–35 cm. In zone 3, the displacement along the negative Z-axis direction is 5–37 cm. In zone 4, the displacement along the negative Z-axis direction is 12.5–32.5 cm, and in zone 5, the displacement ranges from 0 to 25 cm in the negative Z-axis direction. The displacement magnitudes in the Z-direction are significant in all regions.

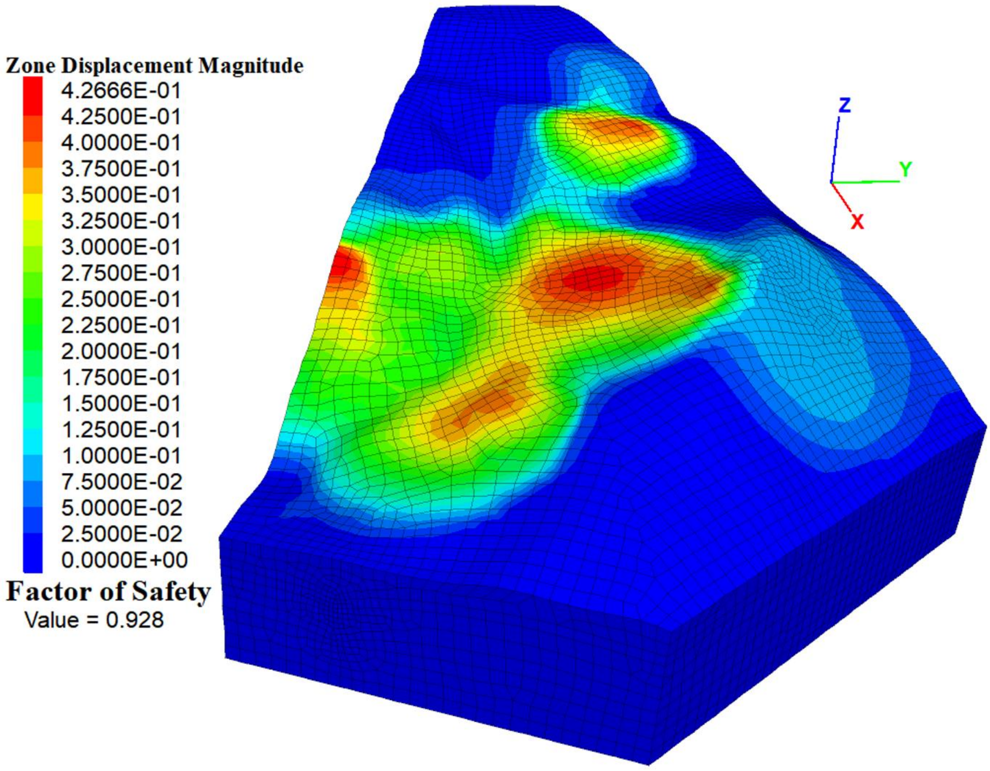

Fig. 16 Slope mass total displacement cloud map

The total displacement contour map of the slope body shows that in zone 1, the total displacement ranges from 0 to 20 cm. In zone 2, the total displacement is between 12.5 and 42.5 cm. In zone 3, the total displacement ranges from 10 to 42.5 cm. In zone 4, the total displacement is between 12.5 and 40 cm. In zone 5, the total displacement ranges from 0 to 35 cm.

Overall, the slope body exhibits a tendency for displacement in the X and Y directions along the slope surface, moving from the higher ridges on both sides towards the lower areas in the central valley. The displacements in each region are primarily in the negative Z-axis direction and are quite substantial, indicating a clear downward sliding trend. The maximum total displacement occurs in the steep slopes of H1 and H2 landslides, specifically in zone 2 and 3. This aligns with the predictive results obtained from ArcGIS and the actual displacements observed during field exploration. From Figure 16, it can be observed that the maximum displacement at the H1 landslide is concentrated on both sides of the Chumeng Highway. This corresponds to the on-site survey findings, where significant sliding occurred on both sides of the road, accompanied by cracks, deformations, and collapses in the vicinity of the road. The safety factor calculated through numerical simulation using FLAC-3D is (K=0.928), indicating that the periphery of the H1 and H2 landslides is distinct. The main cracks at the rear and the sliding walls on both sides have penetrated, indicating that the slope is currently in the sliding phase.

6. Discussion

6.1. Influence of Dynamic Water Pressure

If dynamic water pressure is not considered in Equation (1), the stability factor of the slope would have one less term, the dynamic water pressure, in the denominator. The expression is given by Equation (5)

$$F_s = \frac{c + \left(\left(\left(D-h\right)\gamma_t + h\gamma_s\right) - h\gamma_w\right)\cos^2\theta\tan\varphi}{\left(\left(D-h\right)\gamma_t + h\gamma_s\right)\sin\theta\cos\theta} \tag{6}$$

The critical soil layer thickness derived from Equation (3) is given by

$$D_{cr} = \frac{c}{\cos^2\theta\left(\gamma_s\left(\tan\theta - \tan\varphi\right) + \gamma_w \tan\varphi\right)} \tag{7}$$

This paper considers the effect of dynamic water pressure, and the slope stability factor and critical soil layer thickness calculated with the consideration of dynamic water pressure are relatively lower than those calculated considering only static water pressure. However, under rainfall infiltration conditions, the slope rock and soil mass will be influenced by the dynamic water pressure of the groundwater generated from rainwater. Therefore, considering the effect of dynamic water pressure on the slope rock and soil mass to simulate and analyze the slope stability factor and critical soil layer thickness provides calculation results that are more in line with the actual situation.

6.2. Influence of Topography and Soil Layer Thickness on Model Accuracy

The topography, soil layer thickness, and hydrological characteristics of the slope are crucial for the accuracy of landslide simulation models. The distribution and flow direction of saturated and unsaturated flow within the slope are mainly influenced by the surface topography of the slope and the underlying bedrock. The terrain of the sliding surface between the sliding soil and bedrock is primarily controlled by the surface shape, especially the thickness of the soil layer. The accuracy of the model is significantly affected by the thickness of the soil layer, especially the weathered soil layer. The accuracy and precision of the terrain determine the accuracy of the model.

Detailed topographic data, such as slope and watershed areas, can be obtained through a Digital Elevation Model (DEM). However, information about the thickness of the soil layer and hydrological characteristics over the entire slope or watershed area is relatively scarce and not easy to acquire. In general, shallow instability on the slope often occurs in the terrain areas where excess pore water pressure is generated along the downstream direction of the groundwater flow path in the subsurface soil and rock mass. The subsurface terrain at the soil-bedrock interface is a crucial factor controlling the connectivity of the saturated zone, and the sliding surface of the landslide is influenced by both pore water pressure and the surface terrain of the bedrock. Rainwater infiltrating into the slope soil and transforming into groundwater generates dynamic water pressure. Under this pressure, when water permeates through the pore spaces in the soil, it exerts percolation forces on the surrounding skeleton, proportional to the hydraulic gradient. If the dynamic water pressure points outward from the slope, it will reduce the stability of the landslide body, leading to landslide initiation.

6.3. Influence of Soil-Related Parameters on Model Accuracy

As indicated by Section 4.2, the thickness of the slope soil layer and the topography have a significant impact on the cohesion and internal friction angle of the slope soil mass. Although these parameters can be obtained through field or laboratory analysis, their precise application in practice is challenging, especially considering their spatial variability. The cohesion and internal friction angle of the slope soil mass determine the accuracy of predicting shallow landslides, thus affecting the precision of slope sliding predictions. Additionally, on slopes covered with vegetation, cohesion is equal to the sum of the apparent cohesion between the soil mass and the plant root system. However, calculating the apparent cohesion of the vegetation root system is challenging, and these factors may influence the accuracy of the model.

6.4. Comparison of Predictions, Simulation Results, and Actual Landslide Locations

In the simulation calculations, it was observed that the critical soil layer thickness of the slope units below the Chumeng highway showed a tendency to form continuous patches, indicating that these slope units are likely to experience sliding. Conversely, slope units with uncoupled critical soil layer thickness, due to factors such as the mutual restraint between topography and rock-soil mass and their depth not reaching the critical value for sliding, will not experience large-scale sliding. However, localized surface stripping phenomena may occur.

It is noteworthy that rainfall conditions significantly affect landslide risk, with the number of potential landslide units increasing with the amount of rainfall. Additionally, on steep slopes, the likelihood of sliding is greater due to the smaller maximum soil layer thickness, aligning with observed landslide positions in the field.

Furthermore, through detailed analysis of regions 1 and 2 in Figure 12, we found that their soil layer thicknesses are 2.85m and 11.63m, respectively, leading to significant differences in their stability under rainfall conditions. While the soil layer thickness of region 1 is greater than the critical soil layer thickness but less than the maximum soil layer thickness, it could lead to shallow landslides if the groundwater level rises above the critical groundwater level during rainfall. On the other hand, the soil layer thickness of region 2 is much greater than the maximum soil layer thickness, resulting in sliding regardless of the presence of saturated water flow in the slope.

At the same time, we also observed that the soil layer thicknesses of regions 3, 4, and 5 are 7.15m, 6.03m, and 4.80m, respectively, and these thicknesses fall between the critical and maximum soil layer thicknesses. This implies that, under the influence of the H1 landslide and its own gravitational forces, these regions may experience sliding.

In conclusion, through the above simulation calculations and detailed analysis, we can observe significant landslide risk in the slope units below the Chumeng highway. Especially under rainfall conditions, this risk is further heightened. Therefore, monitoring and preventive measures for these areas are crucial.

7. Conclusion

1)Based on the DEM and soil layer thickness of the slope, a simulation analysis of the slope's stability was conducted. The simulation calculated the critical soil layer thickness of slope units during potential sliding to predict the slope's stability, determining the critical and maximum soil layer thickness when the slope undergoes sliding. This provides a new perspective for the study of slope stability. The positions of instability calculated by the model align with the results of FLAC-3D numerical simulations and field slope sliding conditions, indicating the feasibility of this method.

2)The cohesion and internal friction angle of soil are closely related to the topography and soil layer thickness of the slope. In local areas with steeper slopes, the soil layer thickness is thinner compared to gentler slopes, increasing the likelihood of landslides. The analysis and verification using a slope soil layer thickness model yield results consistent with on-site analysis, demonstrating the feasibility of using the soil layer thickness model to simulate slope stability.

3)This study considered the effect of dynamic water pressure in the critical soil layer thickness model for slopes. Under rainfall infiltration conditions, the rock-soil mass of the slope is affected by the dynamic water pressure generated as rainwater transforms into groundwater. Therefore, considering the dynamic water pressure to simulate and analyze the critical soil layer thickness results in calculations that better match real-world conditions. The cohesion and internal friction angle of slope soil determine the accuracy of predicting shallow landslides. However, their precise application is challenging in practice, especially given their spatial variability.

References

[1] Bandara, R.M.S., Bhasin, R.K., Kjekstad, O., Arambepola, N.M.S.I. (2013). Examples of Cost Effective Practices for Landslide Monitoring for Early Warning in Developing Countries of Asia. In: Margottini, C., Canuti, P., Sassa, K. (eds) Landslide Science and Practice. Springer, Berlin, Heidelberg. https://doi.org/10.1007/978-3-642-31445-2_76

[2] Pardeshi, S. D., Autade, S. E., & Pardeshi, S. S. (2013). Landslide hazard assessment: recent trends and techniques. SpringerPlus, 2, 1-11. https://doi.org/10.1186/2193-1801-2-523

[3] Infante D, Di Martire D, Calcaterra D, Miele P, Scotto di Santolo A, Ramondini M. (2019) Integrated Procedure for Monitoring and Assessment of Linear Infrastructures Safety (I-Pro MONALISA) Affected by Slope Instability. Applied Sciences 5535. https://doi.org/10.3390/app9245535

[4] National Bureau of Statistics, China Statistical Yearbook - 2023, https://www.stats.gov.cn/sj/ndsj/2023/indexch.htm

[5] Das, S.K., Biswal, R.K., Sivakugan, N. et al. (2011) Classification of slopes and prediction of factor of safety using differential evolution neural networks. Environ Earth Sci 64, 201–210. https://doi.org/10.1007/s12665-010-0839-1

[6] Ran, Qh., Su, Dy., Qian, Q. et al. (2012) Physically-based approach to analyze rainfall-triggered landslide using hydraulic gradient as slide direction. J. Zhejiang Univ. Sci. A 13, 943–957. https://doi.org/10.1631/jzus.A1200054

[7] Chen, Y., Zhao, L., Wang, Y. et al. (2019) Precipitation data and their uncertainty as input for rainfall-induced shallow landslide models. Front. Earth Sci. 13, 695–704. https://doi.org/10.1007/s11707-019-0791-7

[8] Bowa, V.M., Kasanda, T. (2020) Wedge Failure Analyses of the Jointed Rock Slope Influenced by Foliations. Geotech Geol Eng 38, 4701–4710. https://doi.org/10.1007/s10706-020-01320-7

[9] Franci, A., Cremonesi, M., Perego, U., Oñate, E., & Crosta, G.. (2020) 3d simulation of vajont disaster. part 2: multi-failure scenarios. Engineering Geology, 279. https://doi.org/10.1016/j.enggeo.2020.105856.

[10] Palazzolo, Nunziarita, David J. Peres, Massimiliano Bordoni, Claudia Meisina, Enrico Creaco, and Antonino Cancelliere. (2021) Improving Spatial Landslide Prediction with 3D Slope Stability Analysis and Genetic Algorithm Optimization: Application to the Oltrepò Pavese Water 13, no. 6: 801. https://doi.org/10.3390/w13060801

[11] Montgomery D R, and Dietrich W E. (1994) A Physically Based Model for the Topographic Control on Shallow Landsliding. Water Resources Research. 1153-1171. https://doi.org/10.1029/93WR02979

[12] Pack, R. T. , Tarboton, D. G. , & Goodwin, C. N. . (1998). The sinmap approach to terrain stability mapping. Congress of the International Association of Engineering Geology, 21--25.

[13] Uchida, T., Tamur, K., Akiyama, K. (2011) THE ROLE OF GRID CELL SIZE, FLOW ROUTING ALGOLITHM AND SPATIAL VARIABILITY OF SOIL DEPTH ON SHALLOW LANDSLIDE PREDICTION. 5th International Conference on Debris-Flow Hazards Mitigation: Mechanics, Prediction and Assessment, Padua, Italy, 2011, 149. https://api.semanticscholar.org/CorpusID:55264970

[14] Borga, M., Dalla Fontana, G., Da Ros, D. et al. (1998) Shallow landslide hazard assessment using a physically based model and digital elevation data. Environmental Geology 35, 81–88. https://doi.org/10.1007/s002540050295

[15] Casadei, M. , Dietrich, W. E. , & Miller, N. L. . (2003). Testing a model for predicting the timing and location of shallow landslide initiation in soil-mantled landscapes. Earth Surface Processes and Landforms: The journal of the British Geomorphological Research Group(9), 28. https://doi.org/10.1002/esp.470

[16] Nguyen, T. T., & Wilson, J. P. (2010, July). Sensitivity of quasi-dynamic topographic wetness index to choice of DEM resolution, flow routing algorithm, and soil variability. In Proceedings of the Ninth International Symposium on Spatial Accuracy Assessment in Natural Resources and the Environmental Sciences (Accuracy 2010), Leicester, United Kingdom.

[17] Pradhan Ananta Man Singh, Kang Hyo Sub, Lee Ji Sung, Tarolli Paolo & Kim Yun Tae. (2016) Shallow landslide hazard modeling by incorporating heavy rainfall statistics and quasi-dynamic wetness index: a case study from Korean mountain. Japanese Geotechnical Society Special Publication(27),1012-1016. DOI:10.3208/jgssp.kor-01

[18] Skempton, A. W., Delory, F. A., (1984) Stability of Natural Slopes in London Clay. SELECTED PAPERS ON SOIL MECHANICS, Thomas Telford Publishing, 70. https://doi.org/10.1680/sposm.02050.0011

[19] Pradel, D. , & Raad, G. . (1993). Effect of permeability on surficial stability of homogeneous slopes. Journal of Geotechnical Engineering, 119(2), 315-332. DOI:10.1061/(ASCE)0733-9410(1993)119:2(315).

[20] Liu C, Wang G, Han W. (2019) Effect of Slip Surface's Continuity on Slope Dynamic Stability Based on Infinite Slope Model. Mathematics. 7(1):58. https://doi.org/10.3390/math7010058

[21] Patton, N.R., Lohse, K.A., Godsey, S.E. et al. (2018) Predicting soil thickness on soil mantled hillslopes. Nat Commun 9, 3329. https://doi.org/10.1038/s41467-018-05743-y

[22] Jang, C. S., Chen, S. K., & Cheng, Y. T. (2016). Spatial estimation of the thickness of low permeability topsoil materials by using a combined ordinary-indicator kriging approach with multiple thresholds. Engineering Geology, 207, 56-65. https://doi.org/10.1016/j.enggeo.2016.04.008.